Optimal Battery Purchasing and Charging Strategy at Electric Vehicle Battery Swap Stations

Bo Sun[a,], Xu Sun[b], Danny H.K. Tsang[a], Ward Whitt[b]

[a]*Department of Electronic and Computer Engineering, The Hong Kong University of Science and Technology, Clear Water Bay, Kowloon, Hong Kong*
[b]*Department of Industrial Engineering and Operations Research, Columbia University, New York, NY, United States*

Abstract

A battery swap station (BSS) is a facility where electric vehicle owners can quickly exchange their depleted battery for a fully-charged one. In order for battery swap to be economically sound, the BSS operator must make a long-term decision on the number of charging bays in the facility, a medium-term decision on the number of batteries in the system, and short-term decisions on when and how many batteries to recharge. In this paper, we introduce a periodic fluid model to describe charging operations at a BSS facing time-varying demand for battery swap and time-varying prices for charging empty batteries, with the objective of finding an optimal battery purchasing and charging policy that best trades off battery investment cost and operating cost including charging cost and cost of customer waiting. We consider a two-stage optimization problem: An optimal amount of battery fluid is identified in the first stage. In the second stage, an optimal charging rule is determined by solving a continuous-time optimal control problem. We characterize the optimal charging policy via Pontryagin's maximum principle and derive an explicit upper bound for the optimal amount of battery fluid which allows us to quantify the joint effect of demand patterns and electricity prices on battery investment decisions. In particular, fewer batteries are needed when the peaks and the troughs of these periodic functions occur at different times.

Keywords: electric vehicles; battery swapping and charging; sustainable transportation; dynamic fluid model; production and inventory control

1. Introduction

Today more and more people are opting for electric vehicles (EVs), as plummeting battery prices and new battery technology have enabled automakers to produce cheaper models with longer ranges. On the horizon, the growth of shared mobility and the emergence of self-driving vehicles strongly complement

---

[*]Corresponding author
  Email address: `bsunaa@connect.ust.hk` (Bo Sun)

EVs, further hastening EV market penetration. In addition, many governments have long incentivized EV purchases, considering numerous environmental and socio-economic benefits. The transition to widespread EV adoption is accelerating, yet there are still concerns centering around (i) long charging times and (ii) grid overloading due to mass EV charging. Charging times are decreasing, due to the emergence of specialized fast-charging facilities, such as Tesla's superchargers that provide up to 135 KW of power and are able to charge a battery to 80% in 45 minutes and to 100% in 75 minutes. But this is not as quickly as consumers would like, as a gas station could serve dozens of cars in that time. Moreover, as EV ranges get longer and batteries get bigger, fast-charge technology is fighting physics. High-power charging could also present grid challenges, as distribution lines and transformers need to handle enormous spikes of electrical demand when cars plug in. A recent Bloomberg report projects global electricity consumption from EVs to rise 300-fold, from 6 TWh in 2016 to $1,800$ TWh by 2040. Additionally, the report warns that the sharp rise in EV ownership could increase pressure on the power network far beyond the current capacity; many systems will have to be replaced or upgraded.

Battery swap, as an alternative refueling option realized in a battery swap station (BSS), is being considered. For example, NIO, a Chinese automobile manufacturer, has recently put 18 BSSs into operation in 14 service areas and plans to deploy $1,100$ additional BSSs by 2020. Battery swap provides a way to address the aforementioned issues associated the rapid charging. First, battery swap provides a more rapid way of refueling EVs and can enable EVs to travel essentially nonstop on long road trips. In addition, empty batteries that are swapped out can be charged when electricity is cheap or demand is low. By controlling the charging time, the potential peak demand or overloading, caused by mass EV charging, can be flattened. Moreover, banks of batteries waiting to be swapped can soak up extra energy and sell it at a profit, thus balancing supply and demand. Battery-swap technologies make it possible to charge batteries with a lower voltage, compared with rapid charging hence should prolong their life expectancy.

1.1. Benefits for Fleet Vehicles

Companies with fleet vehicles may find BSSs especially attractive because one company owns all vehicles and batteries; that is there is no ownership issue about the batteries. For instance, BJEV, the leading new energy electro-mobile producer in China, has built 106 new battery swap stations for electric cabs as of the end of 2017 and planned to build over $3,000$ swapping stations in 100 cities nationwide by 2020. Recently, the company set up a joint venture with Didi Chuxing, China's ride-hailing giant, to work on projects related to ride-hailing, battery swap, and the operation of shared EVs. BJEV estimates that there will be close to 4 million vehicles using the technology with most coming from ride-hailing services. Another example is

Tesla Semi, the company's upcoming all-electric trucks. It is widely speculated a commercial application of these electric trucks may rely on battery-swap technology. According to a third-party analysis, recharging a semi to around 80 percent takes about 90 minutes. Since companies make money by keeping the vehicles on the road, reducing a truck's downtime with a battery swap station can help boost productivity and profits.

With autonomous driving solutions taking care of the driver portion of any trip, charging is yet to be addressed for autonomous vehicles and a battery swap solution could be extremely useful for the hundreds of thousands of shared autonomous EVs that will be flooding streets in the near future. Recent studies regarding the performance characteristics of shared autonomous EV fleets suggest that increasing charging power can reduce the desired fleet size by 30% and the number of chargers by 50%; see Loeb et al. (2018); Bauer et al. (2018). With battery-swap services, it is reasonable to expect that the fleet size and the number of chargers can be further reduced.

1.2. A Preview of the Model

Figure 1 illustrates the daily operations of a BSS. Exogenous demand for battery swap comes from vehicles arriving at the BSS. That demand is fulfilled by exchanging a depleted battery (DB) for a fully-charged battery (FB), but the EV must wait if an FB is not available since an EV with a DB may not have sufficient energy to reach another refueling facility. A BSS can dynamically control the number of DBs to be charged at the same time, which we characterize via the energy consumption rate. Two types of capacity resources constrain the BSS's capability of producing FBs. The number of charging bays restricts the number of DBs that can be charged simultaneously, whereas the number of batteries in the system limits the utilization of the charging bays. These two resources together determine the effective charging capacity of the BSS. Here we regard the number of charging bays as part of long-term planning and take it as given in our model.

Figure 2(a) illustrates the percentage of the average hourly refueling demand of vehicles at gasoline stations over one week. Figure 2(b) shows the energy prices of New York City in Jul. 17-23, 2017, Oct. 17-23, 2017, Jan. 15-21, 2018, and Apr. 16-22, 2018. It is significant that a BSS operates in a highly dynamic time-varying environment. Both the demand rate for battery swap and the price of electricity vary significantly over each day. Indeed, the arrival rate of the residential EV charging demand could have a periodicity where the period is one day (Zhang and Grijalva (2015)). The daily travel patterns are also likely to exhibit periodicity based on the National Household Travel Survey in 2009. [1] The electricity price also

---

[1]The report gathers information about daily travel patterns of different types of households in 2009, and shows that the daily travel statistics are very similar for each weekday and weekend.
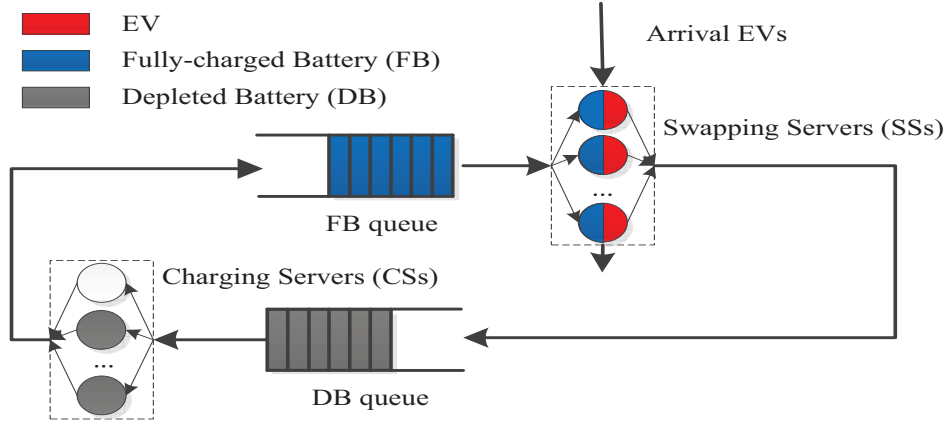
Figure 1: Illustration of a BSS with an infinite-buffer queue for EVs and a closed queue for batteries circulating inside.

exhibits strong daily and weekly periodicity and can often be accurately forecasted, according to Amjady and Keynia (2009). Accordingly, we take the demand rate and the electricity price to be jointly periodic functions in the present study.

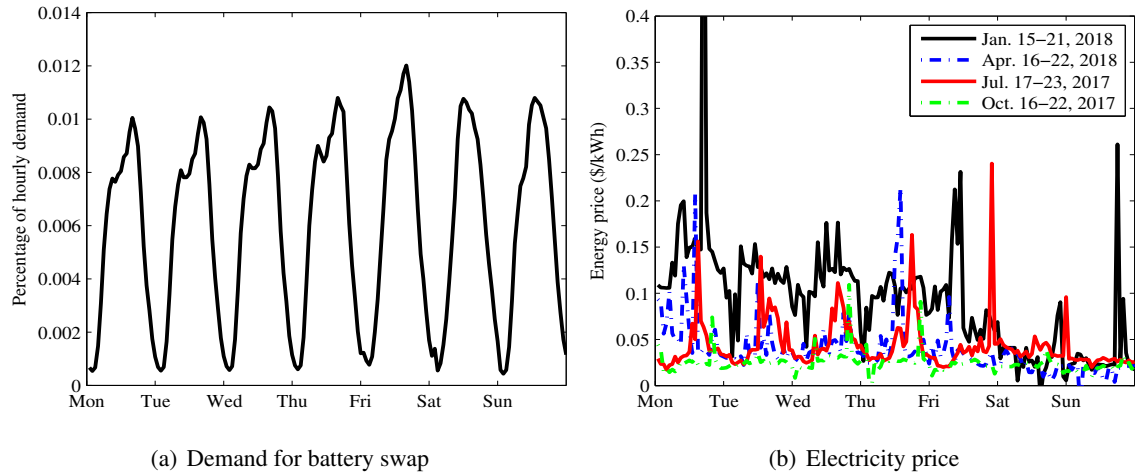(a) Demand for battery swap

(b) Electricity price

Figure 2: Illustrating the battery-swapping demand and the energy price.

As alluded to early, in order for a BSS to run efficiently, the BSS owner not only should know the initial number of batteries to be purchased, but also should perform charging in a time-scheduled fashion on the basis of electricity prices and demand volume. It would clearly be beneficial for the BSS to recharge batteries at full capacity when the electricity price is low in order to cut down on energy cost. On the other hand, high demand for battery swap produces a greater number of DBs that can be used for recharging; hence the BSS owner would also like to recharge batteries when the demand volume is high so as to increase the utilization of the batteries. These conflicting goals suggest that optimization could help to manage a BSS.

4

1.3. Our Contribution

We make four contributions in this paper.

1. We develop a dynamic (time-varying) fluid model that serves as a deterministic and continuous approximation of a large BSS with stochastic arrival of demand and random battery charging times.

2. We propose a fluid-based optimization framework for optimizing battery purchasing and charging operations. Leveraging the fluid-model analysis, we obtain useful managerial insights for optimizing the operations of a BSS under time-varying demand and electricity price: When the degree of similarity between demand and electricity price is high, namely, the high-demand period coinciding with the high-price period, the trade-off between the charging and the waiting cost becomes more salient. (ii) Each additional battery can help mitigate the trade-off, but the marginal gain of doing so decreases in the number of batteries.

3. We propose a variant of the problem that allows to achieve high service levels (i.e., zero waiting). Since the effect of demand uncertainty is more pronounced without backlogs, we introduce a robust optimization formulation to deal with demand uncertainty. We show that the robust formulation is of the same order of complexity as its nominal counterpart.

4. We illustrate through extensive numerical examples the effect of key parameters on the solution to the battery purchasing and charging problem. We identify the key factors that one should focus on in order to improve the performance of a BSS.

The remainder of the paper is structured as follows. In §2, we review related literature. In §3, we introduce our fluid-based optimization framework and provide important analytical results. In §4, we present extensive numerical experiments using real-world data to gain engineering insights. In §5, we present a robust optimization formulation for the optimal charging problem where backlogged demand is not permitted. We draw conclusions and discuss related applications in §6.

2. Literature Review

Our research problem is similar to some inventory control problems, especially the research on a closed-loop supply-chain inventory system in which failed items (DBs) are returned and replaced by functioning ones (FBs), and the returned items are then repaired (recharged) and put back into the inventory. Early work on supply chains with repairable items dates back to the work of Sherbrooke Sherbrooke (1968) where the repair capacity is assumed to be infinite. Extensions of these models with limited repair capacity are sometimes framed as a closed queueing network; see, e.g., Gross et al. (1983); Diaz and Fu (1997). These papers assume the repair cost (if any) to be constant and the demand to be time-stationary and mainly focus

on steady-steady state analysis, whereas we take both the charging cost and the demand (for battery swap) to be time-varying. In addition, the time scale for these inventory problems is drastically different from that for the BSS problem. For repairs the time scale is days or weeks whereas charging times in a BSS tend to be of a much shorter time scale.

Our paper is also related to a fluid approximation of a time-varying stochastic system, which tends to be appropriate for large-scale systems. While the reference list presented here is by no means exhaustive, it should give an indication of the many research studies making use of this technique. The fluid model analysis is often used in the study of queueing and production/inventory systems. Whitt (2006) relies on deterministic fluid models to derive staffing solutions for a call center with uncertain arrival rate and employee absenteeism. The use of fluid model analysis also appears in the revenue management literature. For instance, Maglaras and Meissner (2006) perform a unified analysis of the pricing and capacity control problem in the context of multi-product revenue management and develop a deterministic fluid formulation that gives rise to a closed-form characterization of the optimal control which in turn leads to useful fluid heuristics.

We are by no means the first to consider the battery purchasing and recharging problem for a BSS. A problem that concurrently optimizes the number of batteries and the charging decisions has been formulated and carefully studied by Schneider et al. (2017) under a Markov decision process (MDP) framework. In contrast to their study, we propose a fluid-based optimization framework, inspired by the current implementations of battery-swap technology in China and its potential application to future urban mobility systems. In addition, our fluid-based analysis produces operational insights that can be absent under an MDP framework. Since BSSs are still in the early planning stage, research on optimizing the operation of a BSS remains limited. Mak et al. (2013) analyzes a BSS location problem using a robust optimization approach. Jie et al. (2019) studies a two-echelon capacitated EV routing problem with BSSs to determine the delivery strategy for city logistics. In the paper Tan et al. (2017), the authors model a BSS as a mixed queueing network and analyze the system capacity parameters as the number of batteries approaches infinity. Using the same queueing-theoretic approach, in the paper Sun et al. (2018a), the authors formulate the charging operation problem as a stationary constrained MDP to minimize the charging cost while ensuring a certain quality of service. Widrick et al. (2018) formulates and analyzes a finite-horizon, discrete-time, non-stationary MDP. They consider a scenario, in which the BSS is able to discharge energy back to the power grid, but they do not take into account the cost of waiting due to backlogged demand. In contrast to Widrick et al. (2018), we do not consider discharging operations but take system congestion as an important component in the operating cost. More recently, Sun et al. (2018b) applies a multi-range robust optimization approach to jointly

optimize the location, battery investment and charging strategy for a network of BSSs. They also prohibit backlogged demand and take the recharging time to be the length of one time slot, which oversimplify the charging operations in BSSs based on current battery charging technologies. In addition, as the authors point out, the problem is NP-complete and can be computationally expensive for large-size systems.

Our BSS model is related to EV sharing systems as considered by He et al. (2017). By assuming all customer requests to be lost when there are no available EVs, He et al. (2017) models the EV fleet operations as a closed queueing network. The same modeling approach is adopted by Bellos et al. (2017) to model a car sharing system with a fixed number of vehicles in circulation. In contrast to He et al. (2017) and Bellos et al. (2017), we assume that all unfilled demands will wait in queue instead of being lost. Due to the striking resemblance between these shared transportion systems and the BSS, we believe that the modeling framework provided here can be easily adapted to suit EV fleet management problems.

3. The Fluid-Based Optimization

We start by introducing a dynamic (time-varying) fluid model to describe system dynamics. Fluid is a deterministic divisible quantity. Here we model the state of the battery at a fundamental level. Hence, each quantum of the battery fluid is either fully-charged or depleted. Since the consumption of an FB automatically creates a DB, the total amount of battery fluid is kept a constant. Throughout the rest of this section, we will use κ and b to denote the maximum amount of DB fluid on charging mode and the total battery fluid quantity, respectively. The total EV fluid input (demand for battery swap) over an interval $[0, t]$ is

$$\Lambda(t) \equiv \int_0^t \lambda(u)du, \quad t \geq 0,$$

where $\lambda \equiv \{\lambda(t)|t \geq 0\}$ is the demand (arrival-rate) function. We assume $\lambda(t)$ to be a periodic function in time with the cycle length equal to τ; i.e., $\lambda(t) = \lambda(t + \tau)$. We model the system such that the amount of time for a quantum of fluid to receive a full charge to be *exponentially distributed* with rate parameter μ. This means that the remaining charging time per quantum of DB fluid does not depend on how long time it has been charging; i.e., if the total DB fluid content in the charger is $m(t)$, then the rate at which new FB fluid is produced is $\mu m(t)$. While the exponential distribution may not capture the exact charging-time distribution in practice, it is close to reality since it captures (i) the mean charging times and (ii) the independence between different batteries, and has been used in some known references to model battery charging times; see, e.g., Bayram et al. (2013); Yang et al. (2017); Gnann et al. (2018). The assumption is mostly motivated by mathematical convenience. Indeed, the memoryless property allows us to gain much

analytical tractability which is not possible for other probability distributions. However, to validate the potential implementation of our fluid approach in practice with general charging time distributions, we have numerically shown the effectiveness of the charging solution from our model with exponential charging time distribution even when the charging time is uniformly or deterministically distributed in §3.2.

3.1. System Equations and Problem Formulation

Let $x(t)$ be the state variable representing the amount of FB fluid at time t and $p(t)$ be the electricity price at time t. We assume $p(t)$ to be a periodic function with cycle length τ so that $\lambda(t)$ and $p(t)$ are jointly periodic functions with the same cycle length. We recall there are two types of resource constraints, κ and b, representing the maximum possible amount of DB fluid that can be charged simultaneously and the total amount of battery fluid in circulation, respectively. We use c to denote the waiting cost per unit of time for an EV waiting for service. Further assuming battery investment cost to be γ per unit of time (e.g., if a battery costs \$3,500, or \$350 per year considering a 10% amortization rate, then $\gamma \approx 1$ if we use day as the units of time), we can formulate the BSS battery purchasing and charging problem as

$$\min_{b \geq 0} \quad \underbrace{\gamma \tau b}_{\text{battery cost}} + \underbrace{V(b)}_{\text{operating cost}} , \qquad \text{(first-stage)} \tag{1}$$

where the second-stage problem, which we also refer to as the *charging* problem, is given by

$$V(b) \equiv \min_{x_0 \leq b, m} \int_0^\tau p(t)m(t)dt + c \int_0^\tau x^-(t)dt \tag{2a}$$

$$\text{s.t. } \dot{x}(t) = \mu m(t) - \lambda(t) \qquad 0 \leq t \leq \tau, \tag{2b}$$

$$0 \leq m(t) \leq \kappa \qquad 0 \leq t \leq \tau, \tag{2c}$$

$$m(t) + x^+(t) \leq b \qquad 0 \leq t \leq \tau, \tag{2d}$$

$$x(0) = x(\tau) = x_0. \tag{2e}$$

The goal of the charging problem is to determine a charging policy m^* and an initial FB fluid content x_0^* that minimize the sum of the charging cost and the cost of waiting within one cycle, and we denote its optimal objective value by $V(b)$ so as to indicate the dependence of the solution on the value of b. Here the state variable $x(t)$ can take either positive or negative values. Positive values indicate that we have an amount of $x(t)$ FB fluid in stock whereas negative values occur when demand for FB fluid exceeds its supply in which case there is an amount of $-x(t)$ EV fluid in queue. Constraint (2b) is the basic flow equation derived of conservation laws. Constraint (2c) stems from the fact the amount of charger fluid at any time is nonnegative and cannot exceed the maximum charger fluid κ. Constraint (2d) states that the amount of DB

8

fluid being charged and the amount of FB fluid combined cannot exceed the total amount of battery fluid in system. Finally, we impose the terminal condition (2e) which is primarily motivated by the existence of a periodic-stationary optimal policy π^* to the MDP in Appendix A whose induced FB inventory has a *periodic-stationary distribution*; i.e., x_t equals *in distribution* to $x_{t+\tau}$. Since our fluid model can be seen as a deterministic approximation of the MDP, it would be reasonable to have $x(t) = x(t + \tau)$ in the fluid model with a periodic-stationary control. Loosely speaking, by adding constraint (2e), we restrict ourselves to the space of periodic-stationary solutions.

Note that constraint (2e) requires the amount of FB fluid produced over $[0, \tau]$ to be equal to the demand occurred over the same cycle. Indeed, combining (2b) and (2e) yields

$$\Lambda(\tau) = \mu \int_0^\tau m(t)dt. \tag{3}$$

Further let θ be such that $\mu\kappa\theta = \Lambda(\tau)$, or simply $\theta = \Lambda(\tau)/(\mu\kappa)$. From (2c) and (3), it is readily seen that θ is the minimum amount of time that the BSS has to spend on charging batteries within a cycle. The result below guarantees the existence of an optimal solution over the decision space $\mathbb{R} \times \mathbb{L}$ for the problem specified by (2). The proof makes use of an equivalent formulation and is deferred to the appendix.

Theorem 3.1. *Suppose $\theta \leq \tau$. Then there exists at least one optimal solution (x_0^*, m^*) to the second-stage problem given by (2).*

The next result provides convexity of the charging problem in b, the total amount of battery fluid circulating through the system.

Theorem 3.2. *Under the condition of Theorem 3.1, the function V(b) is convex.*

Proof of Theorem 3.2. It suffices to show for arbitrary b_1 and b_2,

$$V(\varrho b_1 + \bar{\varrho}b_2) \leq \varrho V(b_1) + \bar{\varrho}V(b_2) \quad \text{for} \quad 0 < \varrho < 1 \quad \text{and} \quad \bar{\varrho} \equiv 1 - \varrho.$$

Let $(x_i(0), m_i)$ denote an optimal solution associated with b_i, and let x_i denote the optimal trajectory of the state, $i = 1, 2$. Consider $m \equiv \varrho m_1 + \bar{\varrho}m_2$ and $x \equiv \varrho x_1 + \bar{\varrho}x_2$. We argue that $(x(0), m)$ is feasible for the problem with $b \equiv \varrho b_1 + \bar{\varrho}b_2$. Note that constraints (2b), (2c), and (2e) are trivially satisfied. For the third constraint, we have

$$m(t) + x^+(t) = \varrho m_1(t) + \bar{\varrho}m_2(t) + [\varrho x_1(t) + \bar{\varrho}x_2(t)]^+ \leq \varrho(m_1(t) + x_1^+(t)) + \bar{\varrho}(m_2(t) + x_2^+(t)),$$

where the right-hand side is no greater than $\varrho b_1 + \bar{\varrho} b_2$ which in turn equals b. This shows that constraint (2d) is indeed satisfied and therefore the solution $(x(0), m)$ is feasible. The proof is complete by observing that

$$
\begin{aligned}
V(b) &\leq \int_0^\tau p(t)m(t)dt + c \int_0^\tau x^-(t)dt \\
&\leq \varrho \left(\int_0^\tau p(t)m_1(t)dt + c \int_0^\tau x_1^-(t)dt \right) + \bar{\varrho} \left(\int_0^\tau p(t)m_2(t)dt + c \int_0^\tau x_2^-(t)dt \right) \\
&= \varrho V(b_1) + \bar{\varrho} V(b_2).
\end{aligned}
$$

This shows that the value function $V(b)$ is convex in b. $\qquad\square$

Theorem 3.2 suggests that although adding an additional battery can help reduce the charging and waiting costs altogether, the marginal gain of doing so diminishes. Moreover, Theorem 3.2 shows that the first-stage problem given by (1) is convex and its solution is guaranteed to exist.

3.2. Maximum Principle for the Fluid Optimization

In this section, we characterize the solution to the second-stage problem using Lagrangian form of Pontryagin's maximum principle; see Chapter 3 of Sethi and Thompson (2000); see also Chapter 3 of Bertsekas (1995). To do that, we associate an adjoint function α with equation (2b) and write down the Hamiltonian function

$$
H \equiv H(x(t), m(t), \alpha(t)) \equiv -p(t)m(t) - cx^-(t) + \alpha(t)(\mu m(t) - \lambda(t)). \tag{4}
$$

In (4), we have used the negative of the integrand in (2a), since the minimization of $V(b)$ in (2a) is equivalent to the maximization of $-V(b)$. To apply the Pontryagin's maximum principle, we differentiate (4) to get

$$
\frac{\partial H}{\partial m} = -p + \mu\alpha,
$$

so that the optimal control is of the bang-bang form:

$$
m^* = \begin{cases} 0 & \text{if} \quad p > \mu\alpha, \\ \min(\lambda/\mu, \kappa, b - x^+) & \text{if} \quad p = \mu\alpha, \\ \min(\kappa, b - x^+) & \text{if} \quad p < \mu\alpha. \end{cases} \tag{5}
$$

The adjoint variable $\alpha(t)$ can be interpreted as the future value (at time τ) of one unit of FB at time t. Therefore, the decision rule (5) has a clear economic interpretation: The BSS is willing to charge DB fluid at the maximum (possible) capacity if the marginal benefit of producing an additional FB fluid exceeds the associated cost; similarly, if the marginal benefit falls short of cost, it is beneficial for the BSS not to charge battery at all. To proceed, we form the Lagrangian

$$
L \equiv L(x(t), m(t), \alpha(t), \nu(t)) \equiv H + \nu_1(t)m(t) + \nu_2(t)(\kappa - m(t)) + \nu_3(t)(b - m(t) - x^+(t)), \tag{6}
$$

10

where the set of Lagrange multipliers $\nu \equiv (\nu_1, \nu_2, \nu_3)$ satisfies the complementary slackness (CS) conditions

:

$$\nu_1(t) \geq 0, \quad \nu_1(t)m(t) = 0,$$
$$\nu_2(t) \geq 0, \quad \nu_2(t)(\kappa - m(t)) = 0, \tag{7}$$
$$\nu_3(t) \geq 0, \quad \nu_3(t)(b - m(t) - x^+(t)) = 0.$$

In addition, the optimal state trajectory, optimal control, and the corresponding Lagrange multipliers must satisfy

$$\frac{\partial L}{\partial m} = -p(t) + \mu\alpha(t) + \nu_1(t) - \nu_2(t) - \nu_3(t) = 0 \quad \text{and} \tag{8}$$

$$\dot{\alpha}(t) = -\frac{\partial L}{\partial x} = -c1_{\{x(t)<0\}} + \mu^{-1}\dot{p}(t)1_{\{x(t)=0,-\mu c \leq \dot{p}(t) \leq 0\}} + \nu_3(t)1_{\{x(t)>0\}}. \tag{9}$$

One can easily check by combining the CS conditions (8) and (9) that $\nu_3(t) = \mu\alpha(t) - p(t)$ if $x(t) + m(t) = b$ and $\nu_3(t) = 0$ otherwise.

In canonical control problems, it is usually assumed that the initial state $x(0)$ is fixed. Here the initial state is free but the trajectory must return to it. It turns out that this set-up can be easily handled by using a version of the transversality condition, which involves the values of the adjoint function both at the initial time and at the terminal time. More precisely, this condition requires $(\alpha(0), -\alpha(\tau))$ to be orthogonal to $(x(0), x(\tau))$; see, e.g., equation (4.46) at page 107 in Liberzon (2011). Because (2e) stipulates $x(0) = x(\tau)$, we have

$$\alpha(0) = \alpha(\tau). \tag{10}$$

When the final state is not fixed, there must also be a terminal condition for the adjoint equation. Here that condition is not necessary because we have the extra boundary condition (2e) maintaining the balance between boundary conditions and unknowns. To summarize, the optimal solution (x_0^*, m^*) to the second-stage problem is completely characterized by (2e), (5), and (7) - (10).

We conclude this section by numerically testing the accuracy of the fluid model approximation. To that end, we solve the MDP in Appendix A and the second-stage fluid optimization under the same settings, and then compare the results from the two approaches. To make the problem manageable for the MDP, we run our experiments on a medium-size system with $K = 20$ chargers, $B = 40$ batteries, price function $p(t) = 2.45 - 1.05 \sin(\pi t/12)$ and arrival-rate function $\lambda(t) = 16 - 8 \sin(\pi t/12)$. The cycle length is thus $\tau = 24$ hours. We set the average charging time of each battery to be $1/\mu = 1$ hour and the waiting cost factor to be $c = 0.1$ \$/min/EV. The fluid optimization can be solved fairly quickly by a simple discretization procedure as described in Appendix B. We apply the iterative algorithm in Riis (1965) with a discount factor close to one to compute the optimal policy for the infinite-horizon periodic MDP in Appendix A.

11

(a) Comparing the optimal state trajectory

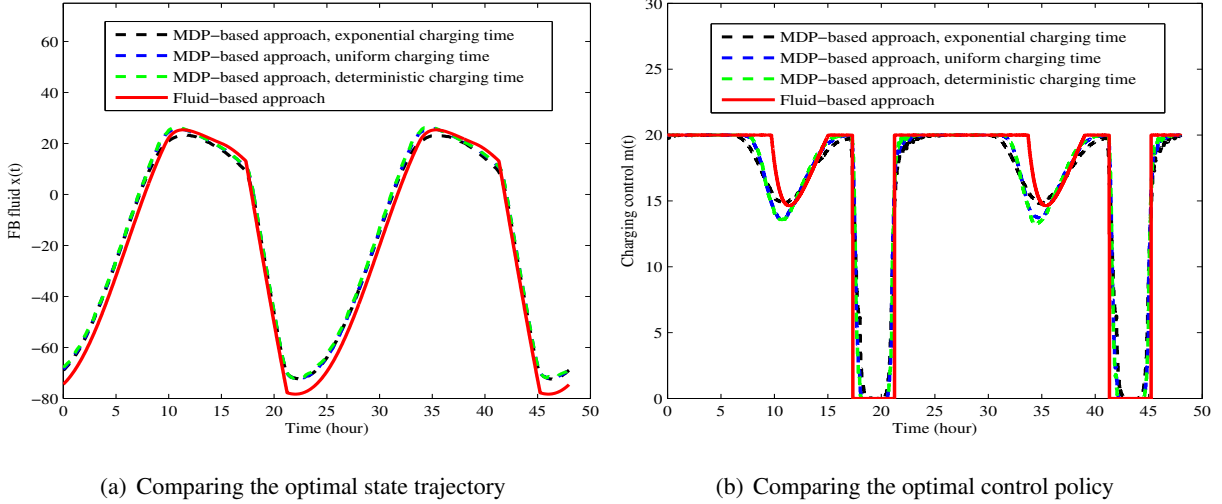(b) Comparing the optimal control policy

Figure 3: Comparison of the fluid-based and MDP-based approaches. The mean charging time of all distributions are set to be the same (i.e., $1/\mu = 1$ hour). The uniform charging time varies within [2/3, 4/3] hours.

This optimal policy is derived by assuming an exponentially distributed battery charging time. To further investigate the impact of charging time distribution on the optimal charging policy, we apply the optimal charging policy to the BSS systems with different charging time distributions, and simulate their mean FB inventory levels and the numbers of working chargers (averaged over 1000 sample paths under the optimal policy from the MDP). We compare those simulated results with the time-varying FB fluid x and the working-charger fluid m computed from the fluid-model approximation in Figure 3. The effectiveness of the fluid-model approximation is visually confirmed from Figure 3, in which both state trajectories and charging controls from MDP-based approach and fluid-based approach are close. Moreover, the simulated results with more general charging time distributions such as uniform and deterministic distributions are also close to fluid-based solution. This verifies that our fluid-based approach can serve as a good approximation to the MDP model even when the charging time is not exponentially distributed.

3.3. Upper-Bound Analysis

To gain greater managerial insights into the joint impact of energy price and demand functions on battery investment cost, here we construct an explicit upper bound for the optimal amount of battery fluid b^* that arises in solving the fluid-based cost minimization problem. We start by focusing on the charging cost. To save on energy costs, the BSS would like to operate at full capacity at those times when the electricity price is among the lowest. To explicitly characterize such a policy, define the set-valued function

$$\phi(\zeta) \equiv \{0 \le t \le \tau : p(t) \le \zeta\}, \tag{11}$$

that maps each real number to a level set. Figure 4 presents a graphical illustration of the function ϕ. From (11) it is easily verifiable that g is a nondecreasing function yet not necessarily continuous. Indeed, if p happens to be a step function, then g has points of discontinuity.
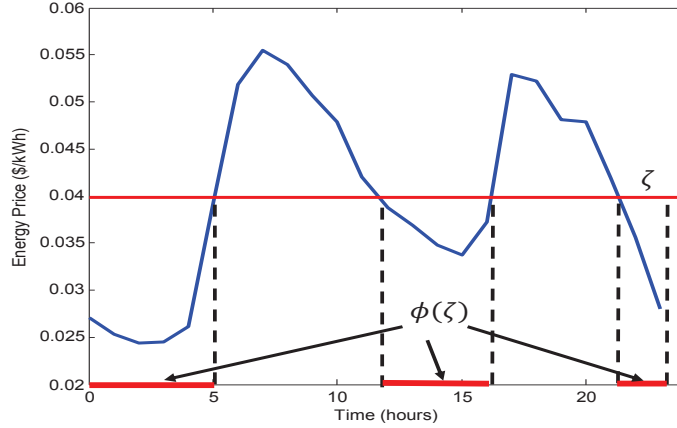

Figure 4: Illustration of the set-valued function $\phi(\cdot)$.

Assumption 3.1. *The price function p is Borel measurable so that $\phi(\zeta)$ given in (11) is a Borel set. Denote by ℓ the Lebesgue measure and define $g(\zeta) \equiv \ell(\phi(\zeta))$. Then there exists a unique $\zeta^* \geq 0$ such that $g(\zeta^*) = \theta$.*

Remark 3.1. *Assumption 3.1 is likely to be violated if the price function is a staircase function. Indeed, in the case of staircase price functions, there typically exist two price levels ζ_1 and ζ_2 such that $g(\zeta_1) \leq \theta \leq g(\zeta_2)$, $\zeta_1 \leq \zeta_2$. To minimize the charging cost, the BSS must charge batteries at full capacity when the price is lower than or equal to ζ_1, and charge the remaining batteries at the price ζ_2. Moreover, there exist multiple charging policies that can achieve the minimum charging cost without loss of demand.*

Suppose for the moment that there is an unlimited amount of battery fluid in the system; i.e., $b = \infty$. Then (2d) is no longer a real constraint. Consider the following charging policy:

$$m^*(t) = \begin{cases} \kappa & \text{if} \quad t \in \phi(\zeta^*), \\ 0 & \text{if} \quad t \notin \phi(\zeta^*), \end{cases} \tag{12}$$

where ζ^* is defined by Assumption 3.1. The result below indicates that m^* is optimal as far as the charging cost is concerned.

Proposition 3.1. *Suppose $\theta \leq \tau$ and Assumption 3.1 holds. If the amount of battery fluid in circulation is unlimited (i.e., $b = \infty$), then the charging policy m^* given in (12) achieves the minimum (possible) charging cost; that is, there exists no such a charging policy that gives a lower charging cost.*

13

We next consider the cost associated with waiting. Note that the cost of waiting will be completely eliminated if we choose $(x(0), m)$ in such a way that

$$x(t) \geq 0 \quad \text{for all} \quad 0 \leq t \leq \tau. \tag{13}$$

Indeed, for a charging policy m, we can choose

$$x(0) \equiv \sup_{0 \leq t \leq \tau} \left[\mu \int_0^t m(u)du - \Lambda(t) \right]^- = \sup_{0 \leq t \leq \tau} \left[\Lambda(t) - \mu \int_0^t m(u)du \right]^+, \tag{14}$$

to ensure that condition (13) holds. To see that this is indeed the case, notice

$$\begin{aligned} x(t) &= x(0) + \mu \int_0^t m(u)du - \Lambda(t) \\ &\geq \left[\mu \int_0^t m(u)du - \Lambda(t) \right]^- + \mu \int_0^t m(u)du - \Lambda(t) \geq 0, \end{aligned} \tag{15}$$

where the first inequality is due to (14) and the second inequality follows from the simple relation $x^+ = x^- + x$. In particular, we set, for the optimal charging policy m^* given in (12)

$$x^*(0) \equiv \sup_{0 \leq t \leq \tau} \left[\Lambda(t) - \mu \int_0^t m^*(u)du \right]^+. \tag{16}$$

By Proposition 3.1 and (15), the solution $(x^*(0), m^*)$ yields the lowest charging cost *without causing any congestion*, provided the total amount of battery fluid in system is sufficient. Therefore, solution $(x^*(0), m^*)$ is optimal for the fluid-model optimization problem given by (2) with $b = \infty$. With the control function m^* and the initial state $x^*(0)$ given by (12) and (16) respectively, the state dynamics, denoted by $x^*(t)$, is uniquely determined by

$$x^*(t) = x^*(0) + \mu \int_0^t m^*(u)du - \Lambda(t), \quad \text{for all} \quad 0 \leq t \leq \tau. \tag{17}$$

Using the state x^* and control m^* specified by (12) and (17) respectively, we define

$$b^* \equiv \sup_{t \leq \tau} \{ m^*(t) + x^*(t) \}. \tag{18}$$

By choosing $b = b^*$, we make sure that constraint (2d) is not violated. Indeed, b^* is the minimum amount of battery fluid content with which both components of the objective function (2a) reach the lowest possible value. The theorem below summarizes the main results in this section.

Theorem 3.3. *Under the conditions of Proposition 3.1, there exists a threshold value b^* such that the value $V(b)$ with respect to b is (i) strictly decreasing for $b < b^*$ and (ii) constant for $b \geq b^*$.*

Theorem 3.3 immediately implies that the objective value of problem (1) is monotonically increasing for $b > b^*$. Consequently, b^* is an upper bound of the optimal amount of battery fluid in the two-stage optimization problem (1). Moreover, this bound depends on the energy price p and demand λ only. To analytically evaluate the joint impact of energy price and demand functions on battery investment cost, we illustrate by an example how the degree of similarity between p and λ can affect the value of b^*. For simplicity, we stipulate that both price and demand follow sinusoidal functions with cycle length τ. Specifically, we assume the price and demand functions to follow

$$p(t) = \bar{p} + A_p \sin(2\pi t/\tau) \quad \text{and} \quad \lambda(t) = \bar{\lambda} + A_\lambda \sin(2\pi(t - \psi)/\tau)$$

, respectively, where $\bar{p}$ and $\bar{\lambda}$ are the vertical shifts, A_p and A_p represent the amplitudes, and ψ denotes the phase shift. Here the degree of similarity between p and λ is quantified by the parameter ψ that serves as an indicator of the degree of synchronization. Note that $\psi = 0$ and $\psi = \tau/2$ represent the cases that demand function is synchronized and unsynchronized with price function, respectively. It is readily checked that the total demand $\Lambda(\tau) = \bar{\lambda}\tau$. In addition, let $\mu = 1$ and $\kappa = 2\bar{\lambda}$. With these parameters, we can calculate the minimum amount of time that the BSS has to spend on charging batteries within a cycle, yielding $\theta = \Lambda(\tau)/\kappa = \tau/2$. Using (12), (16), (17) and (18), we deduce

$$b^* = \kappa + \bar{\lambda}\tau - \int_{\tau/2}^{\tau} \lambda(t)dt = \kappa + \frac{\bar{\lambda}\tau}{2} - A_\lambda \int_{\tau/2}^{\tau} \sin(2\pi(t - \psi)/\tau)dt = 2\bar{\lambda} + \frac{\bar{\lambda}\tau}{2} + \frac{A_\lambda \tau}{\pi} \cos(2\pi\psi/\tau).$$

It is immediate by the analytical expression that b^*, as a function of ψ, attains its maximum at $\psi = 0$, and keeps decreasing until reaching its minimum value at $\psi = \tau/2$. This carries practical implications that are important for the BSS operator to be aware of in order to determine the optimal number of batteries in circulation. In particular, when the demand function and the electricity price function are unsynchronized, the BSS can keep its charging and waiting cost down using a smaller number of batteries. The reason is that when λ is synchronized with p, the BSS tends not to recharge batteries over the high-demand (high-price) period so as to keep its charging cost down, but it has to build high FB inventory over the low-demand (low-price) period to avoid shortages of FBs over the high-demand (high-price) period, which would require a greater number of batteries in system. In contrast, in the unsynchronized case, high price coincides with low demand allowing the BSS to maintain lower FB inventory levels, and hence a smaller number of total batteries.

One way to quantify the degree of similarity of two general vectors/functions is by a scaler ranging from -1 to 1, where -1 and 1 represent the highest and lowest degrees of similarity between the two functions. Specifically, in our context, we use *cosine similarity* as our measurement of the degree of similarity between the general demand function λ and the energy price function p. More formally, we define the cosine

similarity to be

$$\mathcal{C} \equiv \frac{\int_0^\tau \lambda(t)p(t)dt}{\sqrt{\int_0^\tau \lambda^2(t)dt \cdot \int_0^\tau p^2(t)dt}}. \tag{19}$$

It is readily seen that the cosine similarity of two postive functions can never be negative and will range from 0 to 1.

4. Numerical Studies & Discussion

In this section, we numerically solve the two-stage fluid-based cost minimization problem based on real-world data to gain managerial insights into (i) how the optimal charging control trades off the charging and waiting costs in the second-stage problem (2), and (ii) how the number of batteries trades off the battery capital cost and the BSS operating cost in the first-stage problem.

For each first-stage decision variable b, we can solve the second-stage problem by discretization (see Appendix B) as in §1 in Riis (1965), p. 5, and obtain the corresponding second-stage objective value $V(b)$. Then our key problem is to find the optimal b to minimize $\gamma\tau b + V(b)$ in the first-stage problem. By Theorem 3.3, the optimal b is within the interval $[0, b^*]$ where b^* is the upper bound of the optimal battery fluid given in Equation (18). Since a complete enumeration of all feasible b is practically impossible, we approximate the feasible region by a bounded discrete set $\Omega \equiv \{0, 1, \ldots, \lceil b^* \rceil\}$. Moreover, from Theorem 3.2 it follows that the objective function $\gamma\tau b + V(b)$ is convex in b. Therefore, a local optimal value $b^\star$, i.e., $V(b^\star) + \gamma\tau b^\star \leq V(b) + \gamma\tau b$ for $b = b^\star \pm 1$, is also globally optimal in Ω. Thus, we can enumerate $V(b)$ starting from $b = \lceil b^* \rceil$ to 0 until we find the local optimal value $b^\star$.

Although our discussion here is based on the solution to the fluid model optimization, we will interpret b, x and m as the number of batteries in system, the number of FBs and the number of working chargers, respectively. Throughout the section we fix the system parameters as follows: the number of charging bays is $\kappa = 50$, the average charging time is $\mu^{-1} = 1$ hour, the power rate of each charging bay is 26.8 kW. We choose the cycle length τ as one week to take into account the periodicity of price and demand in the time of day and the day of week. Due to lacking the real data of battery-swapping demand, we follow the same data and approach as Widrick et al. (2018) and Nurre et al. (2014), using the refueling demand of vehicles at gasoline stations, as shown in Figure 2(a), to estimate the battery-swapping demand. We assume the demand within each hour follows Poisson process with an average rate determined by the product of the weekly total demand and the hourly demand percentage. We adopt the real energy prices of New York City from LCG Consulting (2018). Specifically, we use the hourly prices as shown in Figure 2(b) to represent the energy prices in summer, autumn, winter and spring. As illustrated in Figure 2(b), the energy prices of

16

weekdays are generally higher than those of weekends due to the electricity load reduction in weekends, and the weekly average prices in summer and winter are higher than those in spring and autumn due to extremely hot/cold weather conditions.

4.1. Trade-offs between the Battery Capital Cost and the BSS Operating Cost

This section studies the first-stage battery purchasing problem (1). To expose the trade-offs between the amortized battery cost $\gamma\tau b$ and the operating cost $V(b)$, we show the operating cost against the battery capital cost with the increase of the number of batteries from 50 to 300 (which is called cost curve in this part) in Figure 5. It can be observed that the marginal reduction of the operating cost decreases with the increase of the battery cost for all cost curves in Figure 5. This observation verifies that $V(b)$ is convex in b as claimed in Theorem 3.2. In the following, we discuss in details about how the key factors affect the trade-offs between battery capital cost and the BSS operating cost in the battery purchasing problem.
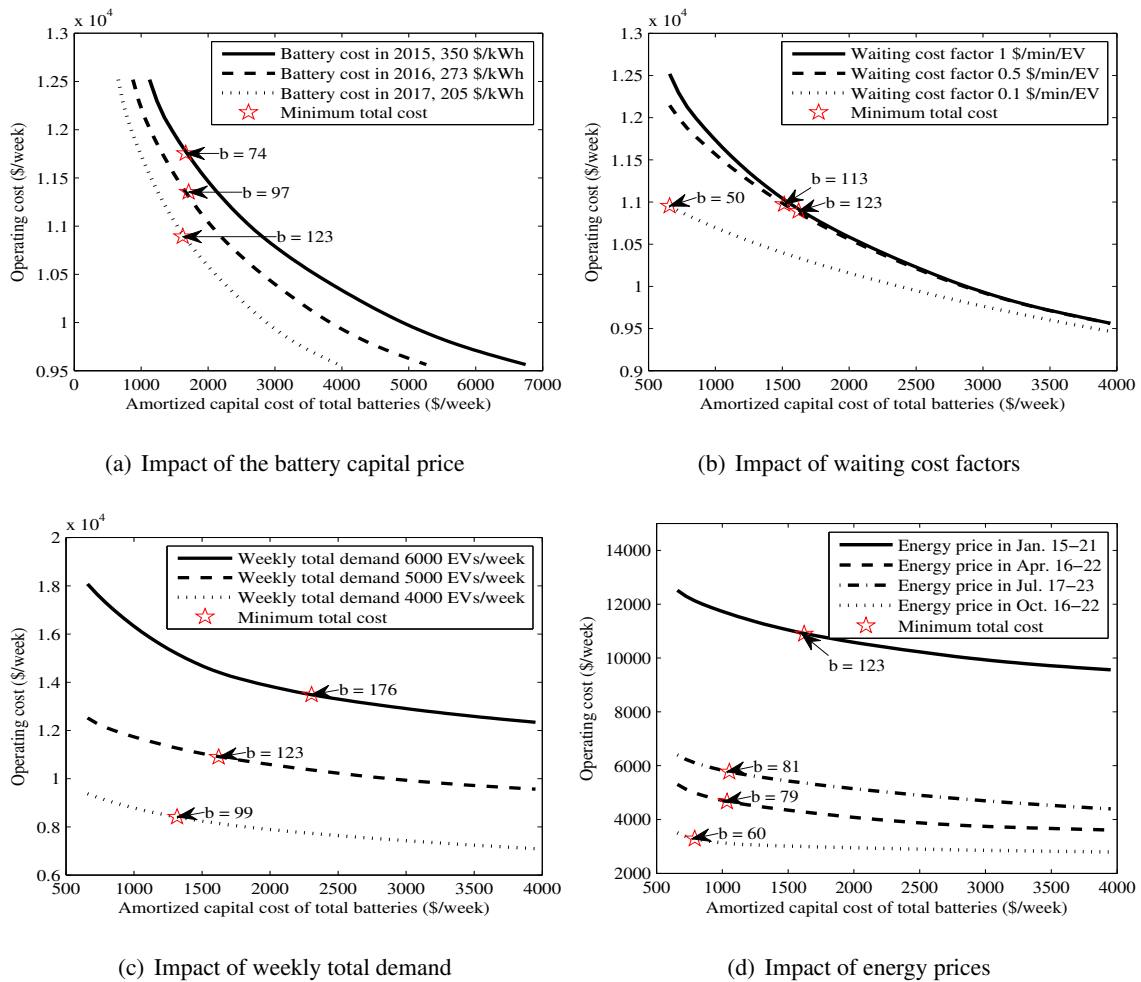

(a) Impact of the battery capital price

(b) Impact of waiting cost factors

(c) Impact of weekly total demand

(d) Impact of energy prices

Figure 5: Illustrating the trade-offs between the battery capital cost and the BSS operating cost.

17

We start with the impact of the battery purchasing cost. Recent years have witnessed the rapid decrease in EV battery price due to the increasing production scale and the advance of the battery manufacturing technology. Battery capital cost (including battery cell and pack costs) has fallen from 1000 $/kWh in 2010 to 209 $/kWh in 2017, see Mark Chediak (2017), and it is expected to reach 125-150 $/kWh around 2025. Because most battery manufacturers are providing eight-year warranties, we assume that each battery has an eight-year lifespan in expectation. Then we can estimate the amortized battery capital cost per week. For example, the amortized cost in 2017 is $26.8 \times 209/8/365 \times 7 = 13.43$ $/week/battery. Figure 5(a) illustrates the cost curves with the battery prices in different years. To single out the effect of battery purchasing cost, we take the electricity price and the demand pattern to be fixed. Note that this keeps the charging cost and the waiting cost unchanged so long as the number of batteries does not change over the years. But we see that the falling battery cost drives the cost curves to the cost-efficient regime (left-bottom corner). Furthermore, the optimal number of batteries to be purchased (i.e., the red star) increases from 74 in 2015 to 123 in 2017. Thus, with the continuously falling battery cost, it becomes more and more cost-efficient to purchase more batteries to reduce the cost.

Next, we fix the battery capital price to be 209 $/kWh, and continue to examine the impact of the key factors that affect the operating cost. Figure 5(b) illustrates the cost curves of different waiting cost factors c given the same price and demand functions. As the waiting cost factor increases, the operating cost increases mainly due to the large increase of charging cost. This is because the BSS has to recharge batteries during the high-price period in order to avoid high waiting cost. Furthermore, to mitigate the negative impact of high penalty due to customer waiting, BSS is also motivated to purchase more batteries. Interestingly, the cost curves for $c = 0.5$ and $c = 1$ are close to each other. A close scrutiny reveals that in these two cases, the number of backlogged demands for battery swap has reached a relatively small value, and hence the waiting cost only takes a small portion of the operating cost. Since the waiting cost indicates the service quality of the BSSs and is the foundation for a successful business, we prioritize the waiting cost over the charging cost for the BSS operations. To do so, we set the waiting cost factor $c = 1$ in the following numerical tests to ensure the service quality.

Figure 5(c) depicts the cost curves with different weekly total demand for battery swap. It can be observed that the marginal gain (in terms of reducing the operating cost) of adding an additional battery is higher when the demand becomes higher. With the increasing penetration of EVs in the future, the battery-swapping demand is expected to increase accordingly. Thus, the BSS operators are encouraged to purchase more batteries to reduce the operating cost in the future. The weekly total demand is set to be 5000 EVs in the following tests to represent a typical penetration of EVs.

Figure 5(d) compares the cost curves when the operating cost is evaluated based on the energy prices in different seasons. It can be observed that the energy prices in different seasons greatly affect the battery purchasing decisions. For prices with a large mean and variation in winter, BSS operators need to maintain 123 batteries in circulation to best trade off the battery cost and the operating cost. However, with a smaller and flatter price in autumn, only 60 batteries are needed to achieve the minimum total cost. To take into account the seasonality of energy prices in the battery purchasing problem, we can reformulate the first-stage problem as follows. We index the four seasons (i.e., winter, spring, summer, and autumn) by $i = 1, \ldots, 4$, respectively. Assume that the operating cost per week in each season can be represented by the periodic-stationary cost in the second-stage problem (2). Then denote the operating cost per week in four seasons by $V_i(b)$, $i = 1, \ldots, 4$. Let ω_i be the ratio of the number of weeks of season i to the total number of weeks of one year. We can determine the optimal number of batteries to be purchased by solving

$$\min_b \quad \sum_{i=1}^{4} \omega_i V_i(b) + \gamma \tau b. \tag{20}$$

Set $\omega_i = 0.25$, $\forall i$. Then based on the energy price data in Figure 2(b), we can solve problem (18) and the optimal number of batteries to be purchased is 81.

To summarize, the seasonality of the operating cost indicates that BSS operators prefer to maintain different number of batteries to minimize their total cost. Thus, instead of purchasing batteries, BSS operators may prefer to lease batteries from companies (which can be independent third-part companies or the battery manufacturing companies) based on the amortized battery cost and adjust the number of batteries in system over different seasons to minimize their overall costs.

4.2. Impact of Demand and Price Functions on the Optimal Charging Control

This section focuses on the second-stage charging operation problem (2) to trade off the charging and waiting costs. In order to reduce the charging cost, the BSS has the incentive to build up FB inventory in low-price periods and then use the on-hand inventory to satisfy the demand in high-price periods. On the other hand, to reduce the waiting cost, the BSS would like to build up FB inventory over underloaded periods (i.e., the time period that $\lambda(t) < \mu\kappa$), and then use the inventory *together with the real-time production of FBs* to satisfy the demand over overload periods. Intuitively, to avoid holding too much FB inventory (which necessarily requires greater number of batteries in circulation), it is beneficial for the BSS to fulfill the demand of overload periods with best effort (i.e., charging at full capacity) rather using the on-hand FB inventory built in the underloaded period only. For this reason, there exists an important trade-off between achieving low charging cost and reducing waiting cost, especially when the overload period is not overlapping with the low-price period.
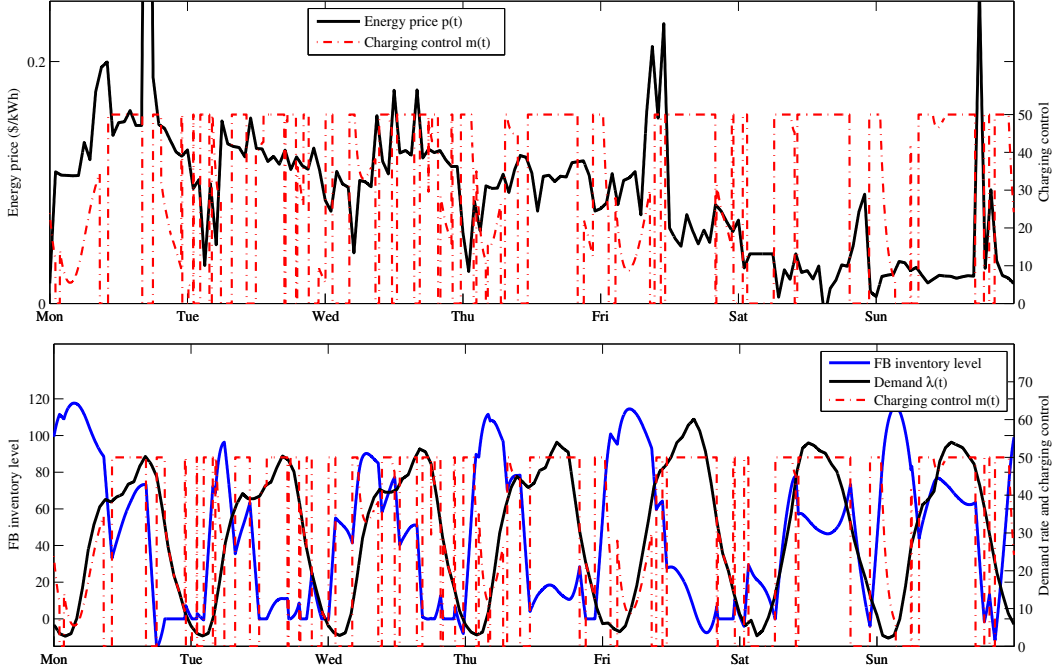
Figure 6: Illustration of the optimal charging control and FB inventory level under the time-varying energy price (Jan. 15-21, 2018) and demand (5000 EVs per week).

We obtain the optimal charging control m and the optimal FB inventory level x by solving the second-stage problem (2). In this numerical test, we set the weekly total demand as 5000 EVs/week, the energy price as the price data of New York City in Jan. 15-21, the waiting cost factor as $c = 1$ \$/min/EV, and total number of batteries as 123. Figure 6 illustrates the optimal charging control with reference to price function, demand function and the FB inventory. Consistent with the optimal charging control (5) derived based on the Maximum Principle, $m(t)$ often, but not always, assumes the maximum or minimum possible values. Thus, we can divide the charging control in Figure 6 into three types of operations: (i) the BSS stops charging when the price is high; (ii) the BSS charges at its maximum capacity $\min\{k, b - x^+\}$ when the price is low; (iii) the BSS charges at the rate of the offered load λ/μ when the price is too high to charge at the maximum capacity but the price decreasing rate $-\dot{p}$ is smaller than the waiting cost factor c, preventing the state variable x transiting to negative values.

We also see that the optimal charging control builds up a large FB inventory before the overload period (i.e., peak of the FB inventory precedes peak of the demand) to reduce the backlogged demand (i.e., the waiting cost) except on Saturday. This is because the energy prices on Saturday and Sunday are much lower than weekdays, and thus to reduce the charging cost the BSS prefers to charge at the full capacity during Saturday to satisfy the demand on the same day. In addition, the low energy prices on weekends motivate

20

the BSS to build up the highest FB inventory before the overload period of Monday to reduce the charging cost.

4.3. Impact of the Degree of Similarity between the Price and Demand Functions on the Operating Cost

(a) Price and demand

(b) Changed operating cost

(c) Cosine similarity
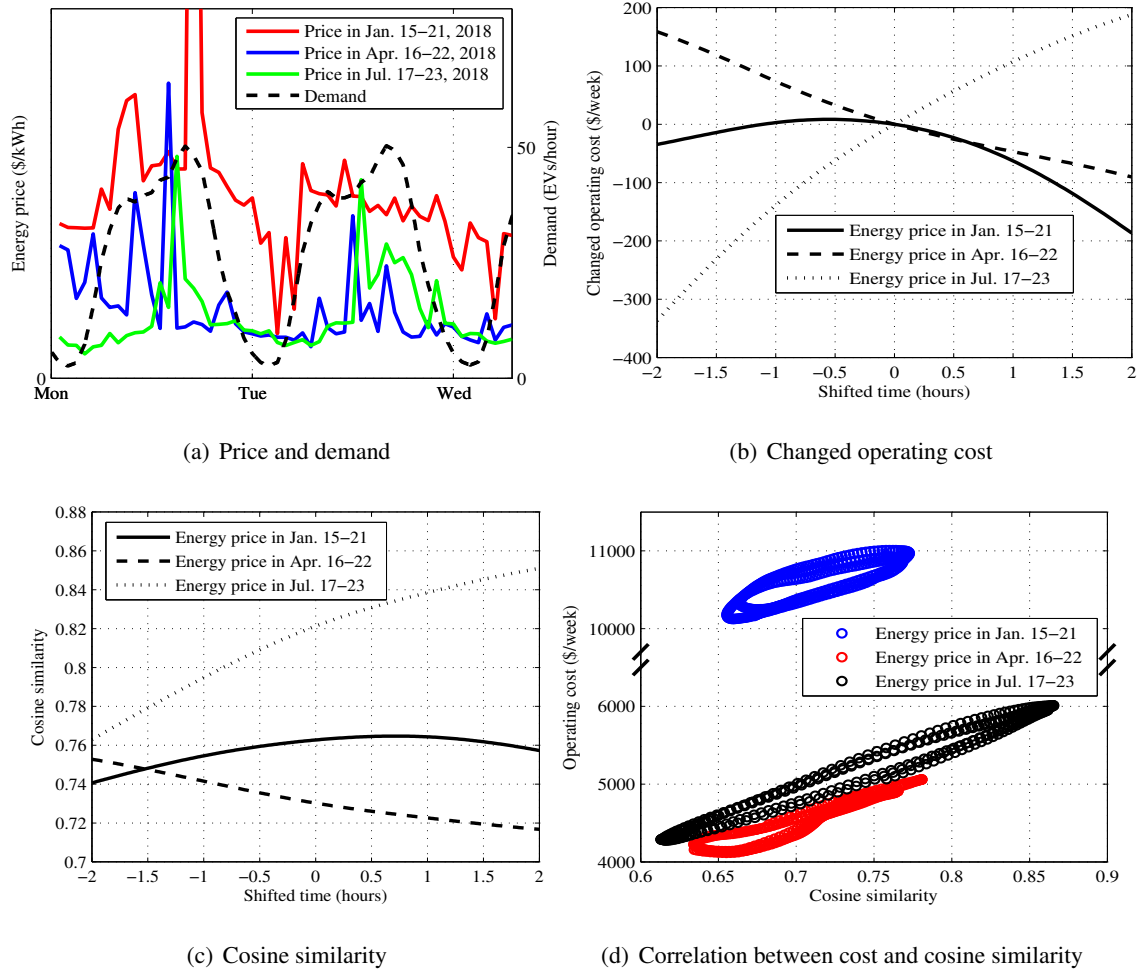
(d) Correlation between cost and cosine similarity

Figure 7: Illustrating operating cost and cosine similarity under different energy price scenarios.

Theorem 3.3 and the example followed show that the degree of similarity between the demand and price functions can greatly affect the upper bound of the optimal number of batteries. Inspired by the this result, we conjecture that given the number of batteries, the degree of similarity can also make a difference in the operating cost. To verify this conjecture, we numerically compute the operating cost when the demand function is shifted over time and compare the resulting cost with that before shifting the demand. We do this numerical test in three scenarios with different energy prices as shown in Figure 7(a). In each scenario, we periodically shift the demand function forward and afterward compared the result to that of the original demand in Figure 7(a). For each shifted demand function, we solve the second-stage problem and obtain

21

the corresponding operating cost. Then we center this operating cost by subtracting the operating cost with that of the original demand function. The change in operating cost is illustrated in Figure 7(b) for different energy price scenarios. We observe that the shifted demand can lead to either increase (positive change in cost) or decrease (negative change in cost) of the operating cost.

We also compute the corresponding cosine similarity, which is defined in Equation (19), between the energy price and shifted demand functions, and show the results in Figure 7(c). We can observe that when the demand is shifted over time, the shifted demand has different degrees of similarity with different energy prices from different seasons. This results in different trends of changed operating cost as shown in Figure 7(b). Particularly, the operating cost tends to fall (rise) when the cosine similarity becomes low (high). Therefore, our conjecture is verified that the operating cost can be reduced when the demand is shifted to be in a lower degree of similarity with the energy price. This phenomenon naturally motivates the introduction of demand-management strategies such as pricing to make demand pattern and energy price less similar. Moreover, we further elaborate the correlation between the degree of similarity and the operating cost by Figure 7(d), in which each point represents the cosine similarity and corresponding operating cost for each pair of energy price and shifted demand functions. We can clearly observe that the operating cost is positively correlated with cosine similarity, which is consistent with our discussions in §3.3. We also notice that a cosine similarity value may correspond to multiple possible operating costs. This is because cosine similarity is a normalized value and may lose some magnitude information when measuring the degree of similarity. Therefore, a particular cosine similarity may correspond to multiple possible pairs of energy price and shifted demand functions, resulting in different operating costs. Since searching for the best measurement for the degree of similarity is out of the scope of this paper, we will leave finding a more proper measurement as our future work.

5. The Charging Problem with no Backlog Permitted

What makes battery swap very attractive is its ability to refuel a vehicle in seconds. This is especially appealing for autonomous cars services, as that make almost nonstop travel possible, minimizing the down time on the road. It is thus sensible to target high service levels, in which case one would want to eliminate customer delays entirely. Clearly, this can be achieved by choosing the waiting cost factor c large enough, in which case the charging problem becomes

$$\min_{(x_0, m) \in \mathcal{X}(b)} \quad \int_0^\tau p(t) m(t) dt \tag{21}$$

22

where the decision region $\mathcal{X}(b)$ for the recourse variables (x_0, m) is specified by

$$\mathcal{X}(b) \equiv \{x_0 \leq b, m : \dot{x}(t) = \mu m(t) - \lambda(t), \quad 0 \leq m(t) \leq \kappa,$$

$$x(t) \geq 0, \quad m(t) + x(t) \leq b, \quad x(0) = x(\tau) = x_0\}. \tag{22}$$

Note that since we impose a nonnegativity constraint on the state variable x, the the component corresponding to the waiting cost in (2a) vanishes.

We remark that the fluid input model is intended to approximate the mean value of the corresponding EV arrival process. In reality, the actual/realized demand process may as well deviate from its mean value. Thus if we were to implement the solution to the fluid-based optimization, we will likely experience a backlog of demand for battery swap in the face of demand uncertainty; an EV may have to wait upon its arrival at the BSS. Below we resort to the idea of robust optimization to deal with uncertain parameters/data.

5.1. A Robust Optimization Formulation

Unlike stochastic optimization that makes distributional assumptions on unknown model parameters, a robust optimization assumes that these quantities belong to certain sets; see, e.g., Bertsimas et al. (2011). In particular, we model demand uncertainty as follows. We use $\lambda(t)$ and $\tilde{\lambda}(t)$ to denote the nominal function and the realization, respectively. In addition, we assume that the realization lies within an interval centered around the nominal function with half-length $\hat{\lambda}(t)$, namely,

$$\left|\tilde{\lambda}(t) - \lambda(t)\right| \leq \hat{\lambda}(t) \quad \text{for all} \quad t \in [0, \tau]. \tag{23}$$

To take into account the fact that the realization is unlikely to be at its worse-case scenario at all times, we introduce a *budget-of-uncertainty function* $\Gamma(\cdot)$, taking value in $[0, \tau]$, and stipulate that

$$\int_0^t \left|\tilde{\lambda}(u) - \lambda(u)\right| du \leq \Gamma(t) \quad \text{for all} \quad t \in [0, \tau]. \tag{24}$$

The function $\Gamma(\cdot)$ allows us to trade off between the level of conservatism of the robust solution and its performance. We take Γ to be a non-decreasing function in t to account for the fact that the aggregate error grows over time.

Let $\mathcal{F}$ denote the uncertainty set, i.e., the set of functions $\tilde{\lambda}$ satisfying (23) and (24). It is quickly verifiable that the function prevents the realization $\tilde{\lambda}(\cdot)$ from being too far away from its nominal value over a large part of the planning horizon. We can spell out the robust optimization formulation that serves as the

robust counterpart of the nominal problem given by (21) and (22).

$$\min_{x_0, m, \chi} \quad \chi$$

$$\text{s.t. } \chi \geq \int_0^\tau p(t)m(t)dt \quad \text{for all} \quad \tilde{\lambda} \in \mathcal{F},$$

$$\dot{\tilde{x}}(t) = \mu m(t) - \tilde{\lambda}(t) \qquad 0 \leq t \leq \tau,$$

$$0 \leq m(t) \leq \kappa, \ \tilde{x}(t) \geq 0 \qquad 0 \leq t \leq \tau, \tag{25}$$

$$m(t) + \tilde{x}(t) \leq b \qquad 0 \leq t \leq \tau,$$

$$\tilde{x}(0) = \tilde{x}(\tau) = x_0.$$

It turns out that the robust optimization formulation can be greatly simplified, yielding an equivalent formulation that shares the same order of complexity as its nominal counterpart given by (21). Specifically, we have the following theorem.

Theorem 5.1. *The robust optimization given by (25) is equivalent to the following problem.*

$$\min_{(x_0, m) \in \mathcal{X}(b)} \quad \int_0^\tau p(t)m(t)dt$$

where the decision region $\mathcal{X}(b)$ for the recourse variables (x_0, m) is specified by

$$\mathcal{X}(b) \equiv \{x_0 \leq b, m : \dot{x}(t) = \mu m(t) - \lambda(t), \quad 0 \leq m(t) \leq \kappa,$$

$$x(t) \geq \eta(t), \quad m(t) + x(t) \leq b - \eta(t), \quad x(0) = x(\tau) = x_0\}, \tag{26}$$

where

$$\eta(t) \equiv \min\left\{\Gamma(t), \int_0^t \hat{\lambda}(u)du\right\} \quad \text{for} \quad 0 \leq t \leq \tau.$$

In this formulation, the demand uncertainty has an effect only on the no-backlog constraint and the upper limit on the number of batteries either fully charged or being charged. In other words, the uncertainty of demand translates into protection levels for the FB inventory; i.e., the protection levels guarantee that the FB inventory remains positive and depend on the budget-of-uncertainty function Γ and the variation parameter $\hat{\lambda}$ for the demand function λ, which are determined through the solution to the dual problem (C.13).

5.2. Impact of Demand Uncertainty on Battery Capital Cost and BSS Operating Cost

Finally, we study the impact of the demand uncertainty on the battery purchasing cost and operating cost when no backlog is permitted for high service levels. To specify the uncertainty set, we let $\hat{\lambda}(t) = \sigma\lambda(t)$. Then combining with (23), we have $(1 - \sigma)\lambda(t) \leq \tilde{\lambda}(t) \leq (1 + \sigma)\lambda(t)$, $0 \leq t \leq \tau$, which restricts the demand realization to be around the nominal demand with at most σ error. This uncertainty bound is

(a) Uncertainty bound of demand function with $\sigma = 0.1$ (b) Protection levels with $\sigma = 0.1$
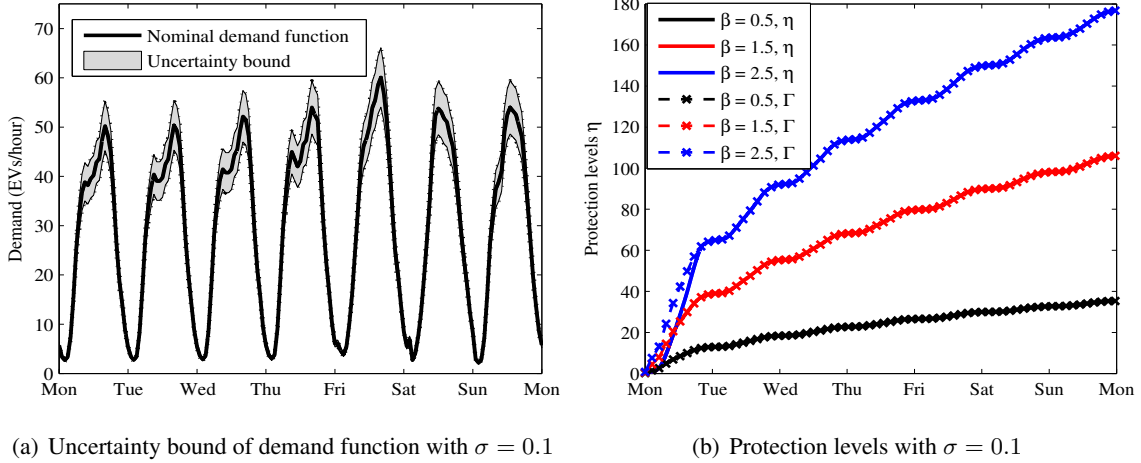
Figure 8: Illustrating the uncertainty bound and the resulting protection levels with different robustness factors.

illustrated in Figure 8(a). Next, we set the budget-of-uncertainty function $\Gamma(t) = \beta\sqrt{\int_0^t \lambda(u)du}$. Here our choice of Γ is primarily inspired by the functional central limit theorem satisfied by non-homogenous Poisson arrival process; see, e.g., Kurtz et al. (1978) lemma 3.1. Together with (24), we have

$$\left|\int_0^t \tilde{\lambda}(u)du - \int_0^t \lambda(u)du\right| \leq \int_0^t \left|\tilde{\lambda}(u) - \lambda(u)\right| du \leq \beta\sqrt{\int_0^t \lambda(u)du} \quad \text{for all} \quad t \in [0, \tau]. \tag{27}$$

Thus, the cumulative realized demand up to time t is around the cumulative nominal demand and does not deviate from it beyond a squared-root term. Here σ is a problem-specific parameter and β is an adjustable factor that controls the level of robustness in the robust second-stage problem. A larger σ or β indicates a higher level of uncertainty, and hence the corresponding solution is more conservative. We solve this robust optimization problem based on the reformulation specified by Theorem 5.1. Recall that the uncertainty set determined by both σ and β is finally transformed into protection level η, which affects the battery purchasing cost and operating cost. The protection levels with varying robustness factors β and fixed variation parameter $\sigma = 0.1$ are shown in Figure 8(b). We notice that protection level η is dominated by Γ in most cases except when the robustness factor is set to be a very large value $\beta = 2.5$. This is because the realization of the demand is unlikely to always take the worse-case values (i.e., $(1+\sigma)\lambda(t)$ or $(1-\sigma)\lambda(t)$). Therefore, the budget-of-uncertainty function $\Gamma(t)$ is often less than the cumulative error function $\int_0^t \hat{\lambda}(u)du$, and hence dominates the determination of protection levels. Figure 9(a) and Figure 9(b) show the battery purchasing cost and operating cost as a function of robustness factor β and variation parameter σ, respectively. It can be observed that with the increase of β or σ, battery purchasing cost keeps increasing because more batteries are needed to avoid violating the constraints enhanced by protection levels, which increase with β and σ. Meanwhile, the operating cost keeps decreasing with β and σ because the increasing number of

batteries offers more flexibilities for batteries to charge in low-price periods, and thus reduces the operating cost. However, the total cost of battery purchasing and operating cost still keeps increasing as one pursues a more robust solution. Also notice that the battery cost and operating cost become nearly unchanged after σ reaches 0.05 in Figure 9(b). This is because the protection levels start to be dominated by Γ, and the increase of variation parameter nearly has no impact on the cost.
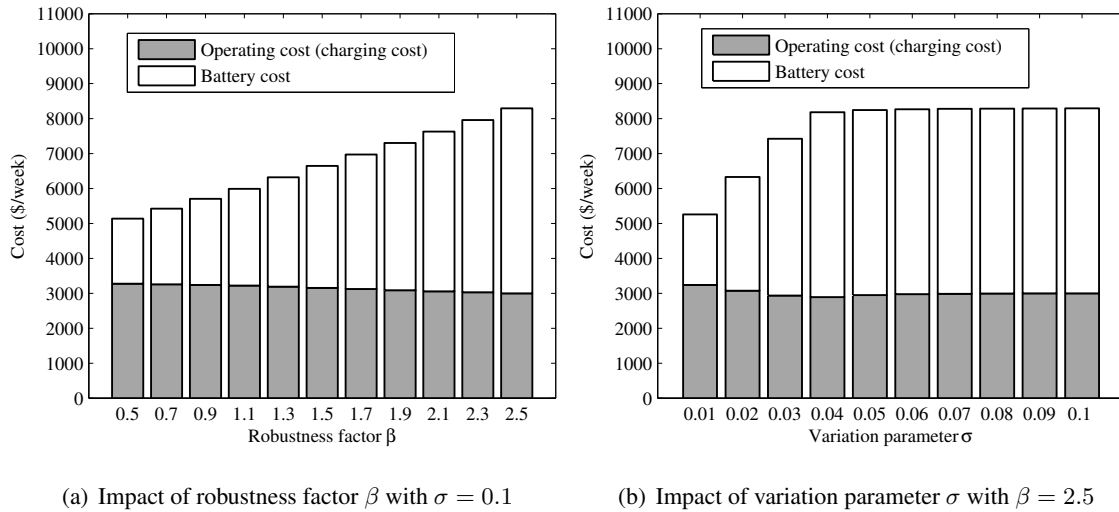

(a) Impact of robustness factor β with $\sigma = 0.1$ (b) Impact of variation parameter σ with $\beta = 2.5$

Figure 9: Illustrating the impact of robustness factor β and variation parameter σ on battery purchasing cost and operating cost.

6. Conclusions

In this paper we studied the problem of battery purchasing and charging at an EV BSS. Based on the fluid model analysis, we gained important managerial insights for determining medium-term decisions (i.e., minimum number of batteries) and how system parameters affect the optimal charging policy. We found that it is tremendously helpful for the BSS to run in an environment where the demand and the electricity price function are *asynchronous*. Particularly, when the demand function is out of sync with the price function, charging at full capacity during the low-price period can reduce both charging cost and cost of waiting at the same time. In contrast, when the demand and the price function are highly synchronous, it becomes difficult to achieve low charging cost and low cost of waiting at the same time. This leads us to the consideration of demand management that complements the supply management view adopted by the present paper.

Although motivated by EV BSS operations, our model can be directly applied to BSSs for electric scooters. For example, Gogoro, a Taiwan-based electric scooter manufacturer, operates more than 500 BSSs across the region, with approximately 69, 000 batteries swapped per day. A system at this scale evidently fits in with our fluid-based framework. Our approach may also be applied to other systems that share common

features with a BSS. One example is a bike-sharing system that pays some of its members to redistribute the bikes themselves so as to resolve the "rebalancing problem", in which riders overload a system's most popular takeoff points and destinations, rendering docks useless (Chung et al. (2018)). Specifically, consider an idealized model with two bike locations A and B connected by a one-way street with direction from A and B. One can draw an analogy between these two models by regarding each bike as a battery and each pick-up at location A as an EV arrival. Then each reverse trip (from B to A) corresponds to a charge completion for the BSS. Moreover, the transit time from A to B and that from B to A can be thought of as the battery-swapping and battery charging times, respectively. Yet the forms of controls used are slightly different. A bike-sharing system influences its number of reverse commuters indirectly by dynamically adjusting its rewards whereas a BSS can decide the number of working chargers directly.

7. Acknowledgement

Appendix A. An MDP-Based Formulation

Throughout Appendix Appendix A, we will use K and B to denote the numbers of charging bays and batteries to distinghish them from their couterparts κ and b in the fluid model. We first describe the second-stage problem and present the first-stage problem thereafter.

Appendix A.1. The Second-Stage Problem

Under the MDP framework, the action taken at each decision epoch is the number of DBs to be put in the charging bays and start charging. The objective of the MDP is to find a policy for charging batteries that can best trade off the charging cost and the cost of waiting. We adopt a discrete-time formulation where time is discretized into small slots of length δ, indexed by $k = 1, 2, \ldots$. To capture the fact that demand and electricity price depend on the time of day and the day of the week, we allow the parameters in both state transition probability and one-slot cost function to be time-varying. Specifically, we assume that the number of EV arrivals over the k-th slot $[k\delta, (k+1)\delta]$, denoted by ξ_k, to be a Bernoulli random variable with parameter $\lambda_k \delta$. Here we assume $\{\lambda_k; k \geq 0\}$ to be a periodic sequence with cycle length τ, i.e., $\lambda_k = \lambda_{k+\tau}$ for any k. With slight abuse of notation, we write λ_k in place of $\lambda_k \delta$ and refer to λ_k as either the demand rate or probability of arrival in slot k. We model the system such that the amount of time for a DB to receive

a full charge is geometrically distributed with parameter $\mu\delta$. Again, with slight abuse of notation, we write μ in place of $\mu\delta$ and refer to μ as either the charging rate or the probability that a battery finishes charging during the slot.

The sequence of events in each time slot is as follows. At the beginning of slot k, batteries that receive a full charge become available and backlogged demand (if any) for battery swap is fulfilled immediately from on-hand FBs. Then the system operator observes the system state and electricity price p_k, and decides how many batteries to start charging. Here we assume $\{p_k; k \geq 0\}$ to be a periodic sequence as well with the cycle length equal to τ, i.e., $p_k = p_{k+\tau}$ for all k. Thus $\{\lambda_k; k \geq 0\}$ and $\{p_k; k \geq 0\}$ are jointly periodic with a common cycle length τ. At the end of the slot, the demand ξ_k is realized, and finally the charging and waiting costs are incurred. We now mathematically characterize the MDP using the notation introduced above.

1. The state of the system in slot k, $x_k \in \mathcal{X} \equiv \{-\infty, \ldots, -1, 0, 1, \ldots, B\}$ represents the inventory level of FBs at the beginning of period k. Here, a positive value indicates the existence of FBs in system and a negative value is understood to be backlogged demand. Thus, the number of DBs at time slot k equals $B - x_k^+$, where x^+ denotes the positive part of x, i.e., $x^+ \equiv \max(x, 0)$.

2. The action taken at the beginning of the k-th slot, $a_k \in \mathcal{A}_k(x_k) \equiv \{0, 1, \ldots, \min(B - x_k^+, K)\}$, is the number of DBs placed in the charging bays. A decision rule, $\pi_k : \mathcal{X} \to \mathcal{A}_k(x_k)$, is a function mapping from the state space $\mathcal{X}$ to the action space $\mathcal{A}_k(x_k)$, which indicates how the system operator selects an action $a_k \in \mathcal{A}_k(x_k)$ at a decision epoch k when the system state is $x_k \in \mathcal{X}$. Because the decision rules depend on the current system state only rather than the entire history, we are essentially restricting ourselves to Markovian decision rules. We use $\pi \equiv (\pi_1(x_1), \pi_2(x_2), \ldots)$ to denote a policy specifying the decision at all decision epochs. Since we consider a periodic system, we anticipate that both the state and the optimal control policy should exhibit time-periodic structure as well, namely, $x_k = x_{k+\tau}$ and $\pi_k(x_k) = \pi_{k+\tau}(x_{k+\tau})$, which will be rigorously shown in Theorem A.1. Denote by Π the set of the deterministic periodic-stationary policies.

3. We denote by $q_k(j|x_k, a_k)$ the transition probability that the system state reaches j at time $k+1$ from x_k when action a_k is taken. Let $\eta_k \equiv \eta_k(a_k)$ denote the number of batteries that *become* fully-charged at the beginning of the $(k+1)$-th slot. From our distributional assumption on the charging times, it can be verified easily that η_k is a binomial random variable with parameters (a_k, μ). The transition equation for the state is then given by

$$x_{k+1} = x_k - \xi_k + \eta_k. \tag{A.1}$$

It is readily checked from (A.1)

$$q_k(j|x_k, a_k) = \begin{cases} \lambda_k f_b(0; a_k, \mu) & \text{if} \quad j = x_k - 1, \\ \lambda_k f_b(j - x_k + 1; a_k, \mu) + (1 - \lambda_k) f_b(j - x_k; a_k, \mu) \\ \quad \text{if} \quad x_k \le j < x_k + a_k, \\ (1 - \lambda_k) f_b(a_k; a_k, \mu) & \text{if} \quad j = x_k + a_k, \end{cases} \tag{A.2}$$

for $f_b(k; n, p)$ being the probability mass function of a binomial distribution with parameters (n, p).

4. The one-slot cost when action a_k is taken in state x_k at time k that leads to transition to x_{k+1} at time $k + 1$ is the cost of system incurred over the k-th slot, given by

$$c_k \equiv c_k(x_k, a_k) = pa_k + cx_k^-, \tag{A.3}$$

where we have written p_k and c in place of $p_k\delta$ and $c\delta$, respectively, similar to what we did with $\lambda_k\delta$ and $\mu\delta$, and x^- denotes the negative part of x, i.e., $x^- \equiv \max(-x, 0)$. Here x_k^- represents the backlog, namely, the number of EVs waiting for battery swap, p is the charging cost per battery per unit time, c is the cost of waiting per EV in queue per unit time.

5. As we will be primarily interested in minimizing long-run average cost, we choose to present the infinite-horizon average-cost formulation. For simplicity, we suppose that the initial system state is zero. Let c_k^π denote one-slot cost at time k under policy π, and $C(\pi) \equiv \limsup_{T\to\infty} T^{-1} \sum_{k=1}^{T} c_k^\pi$ denote the corresponding long-run average cost, where T is the time horizon. Then the infinite-horizon cost-minimization problem can be formulated as

$$\inf_{\pi\in\Pi} C(\pi) \equiv \inf_{\pi\in\Pi} \left(\limsup_{T\to\infty} T^{-1} \sum_{k=1}^{T} c_k^\pi \right). \tag{A.4}$$

The result below guarantees the existence of a periodic-stationary optimal policy.

Theorem A.1. There exists a periodic-stationary optimal policy π^* for problem (A.4); i.e., the decision rule π^* at time $k = j\tau + i$ ($j \in \mathbb{Z}^+$ and $i \le \tau$) is independent of j but depends on i.

Proof of Theorem A.1. The key is to show the periodic MDP can be reformulated so as to be stationary. This is done by enlarging the state and the action space. Define $\bar{\mathcal{X}} \equiv \{(x, k); x \in \mathcal{X}, k \in \{1, \ldots, \tau\}\}$ and $\bar{\mathcal{A}} \equiv \{(a, k); a \in \mathcal{A}_k, k \in \{1, \ldots, \tau\}\}$. Let $\bar{c}((x, k), (a, k)) = c_k(x, a)$, and let $\bar{q}(\cdot|(x, k), (a, k))$ assign probability one to $\mathcal{X} \times \{k + 1\}$ for $k \neq 0 \pmod{\tau}$ and to $\mathcal{X} \times \{1\}$ for $k = 0 \pmod{\tau}$ with the marginal distribution of the first coordinate being $q_k(\cdot|x, a)$. Then the MDP with state space $\bar{\mathcal{X}}$, action space $\bar{\mathcal{A}}$, cost structure $\bar{c}$, and transition law $\bar{q}$ is time-stationary. Because the original action space $\mathcal{A}$ has finite elements, the new action space $\bar{\mathcal{A}}$ is finite and hence compact. An application of Theorem 3.8 in Schäl (1993) (see the

references there for earlier related work) allows us to conclude the existence of a stationary optimal policy for the reformulated MDP. By the earlier transformation of the state and the action space, we conclude that there exists a periodic-stationary optimal policy π^* for problem (A.4). □

Appendix A.2. The First-Stage Problem

Note that the solution to the MDP relies on the "fixed parameter" B. Following the convention, we use $V(B)$ to denote the optimal objective value. On the one hand, increasing B allows us to achieve lower objective value $V(B)$. On the other hand, EV batteries are expensive to manufacture. We thus incorporate costs of capital and assume battery investment cost to be γ per unit of time. For example, if a battery costs \$3,500, or \$350 per year considering a 10% amortization rate, then $\gamma \approx 1$ if we use day as the units of time. Our first-stage problem is then formulated as follows:

$$\min_B V(B)\tau + \gamma\tau B. \tag{A.5}$$

Appendix B. Discrete-time Approximation of the Fluid Model

We turn the second-stage cost minimization problem (2a) - (2e) into a convex program by discretization. Let Δt denote a small time interval and $N = \tau/\Delta t$ denote the total number of time intervals within a cycle $[0, \tau]$. Let $k \in \{1, \ldots, N\}$ be the index of the time intervals. Then we have $m \equiv \{m(k); k = 1, \ldots, N\}$ representing the working-charger fluid during time interval k. Additionally, let $x \equiv \{x(k); k = 0, 1, \ldots, N\}$, where $x(k)$ denotes the amount of FB fluid at the end of the time interval k when $k = 1, \ldots, N$ and $x(0)$ denotes the initial FB fluid at the beginning of the first time interval. We can discretize (2a) - (2e) as follows.

$$
\begin{aligned}
\min \quad & \sum_{k=1}^{N} p(k)m(k)\Delta t + c\sum_{k=1}^{N}[x(k)]^-\Delta t, \\
\text{s.t.} \quad & x(k) - x(k-1) = \mu m(k)\Delta t - \lambda(k)\Delta t, \qquad k = 1, \ldots, N, \\
& 0 \leq m(k) \leq \kappa, \qquad k = 1, \ldots, N, \\
& m(k) + [x(k)]^+ \leq b, \qquad k = 1, \ldots, N, \\
& x(0) = x(N).
\end{aligned}
\tag{B.1}
$$

Appendix C. Technical Proofs

Proof of Theorem 3.1. For the ease of mathematical analysis, we turn the original fluid-model optimization into an equivalent problem. Loosely speaking, two optimization problems are equivalent if an optimal

solution to one can easily be "translated" into an optimal solution for the other. Here we substitute (2b) into the objective (2a) and constraints (2c) - (2d) to get

$$\min_{x \in \mathbb{C}_1} \quad \mu^{-1} \int_0^\tau p(t)(\lambda(t) + \dot{x}(t))dt + c \int_0^\tau x^-(t)dt, \tag{C.1}$$

$$\text{s.t.} \quad 0 \leq \mu^{-1}(\lambda(t) + \dot{x}(t)) \leq \kappa, \qquad 0 \leq t \leq \tau, \tag{C.2}$$

$$\mu^{-1}(\lambda(t) + \dot{x}(t)) + x^+(t) \leq b, \qquad 0 \leq t \leq \tau, \tag{C.3}$$

$$x(0) = x(\tau), \tag{C.4}$$

where we have used $\mathbb{C}_1$ to denote the space of differentiable functions over $[0, \tau]$. The rest of the proof proceeds in two steps. We first show that the equivalent problem specified by (C.1) - (C.4) is a convex optimization problem. We then argue that we are minimizing over a compact set of continuous functions. Noting that there exists at least one optimal solution to a convex optimization problem over a compact set (see, e.g., Beck (2014), p. 149), we complete the proof.

Let us define $\mathcal{F}^+ : \mathbb{C} \to \mathbb{C}, x \mapsto x^+$ and $\mathcal{F}^- : \mathbb{C} \to \mathbb{C}, x \mapsto x^-$ to be two mappings from the space of continuous functions $\mathbb{C}$ to itself. It is evident that both $\mathcal{F}^+$ and $\mathcal{F}^-$ are convex. Also define $\mathcal{A} : \mathbb{C}_1 \to \mathbb{L}, x \mapsto \mu^{-1}(\lambda + \dot{x})$. It is immediate that $\mathcal{A}$ is affine and hence convex. Next define

$$\mathcal{G} : \mathbb{L} \to \mathbb{R}, y \mapsto \int_0^\tau p(u)y(u)du \quad \text{and} \quad \mathcal{H} : \mathbb{C} \to \mathbb{R}, x \mapsto \int_0^\tau x(u)du.$$

That $\mathcal{G}$ and $\mathcal{H}$ are linear mappings implies they are convex. Finally, let us use $\mathcal{P}_t : \mathbb{C} \to \mathbb{R}, x \mapsto x(t)$ to denote the projection mapping at time t. The objective (C.1) is convex in x due to the fact that $\mathcal{G} \circ \mathcal{A} + \mathcal{H} \circ \mathcal{F}^-$ is convex. Similarly, we can write (C.2), (C.3) and (C.4) as $0 \leq \mathcal{A}(x) \leq \kappa$, $(\mathcal{A} + \mathcal{F}^+)(x) \leq b$ and $(\mathcal{P}_0 - \mathcal{P}_\tau)(x) = 0$ respectively. Hence all constraints are convex.

To argue that the feasible regime $\mathbb{X}$ is compact, we apply Arzela-Ascoli theorem. To that end, we show that (i) functions in $\mathbb{X}$ are uniformly bounded, and (ii) they are *equicontinuous*, i.e., for every $\epsilon > 0$, there exists $\delta > 0$ such that $|x(t) - x(s)| < \epsilon$ uniformly over $\mathbb{X}$ whenever $|t - s| < \delta$. From (C.3), it follows $-\lambda^\uparrow \leq \dot{x} \leq \mu(\kappa - \lambda^\downarrow)$ where $\lambda^\uparrow \equiv \sup_{0 \leq t \leq \tau} \lambda(t)$ and $\lambda^\downarrow \equiv \inf_{0 \leq t \leq \tau} \lambda(t)$. Hence, condition (ii) is automatically satisfied. By the same token, condition (i) reduces to the statement that $x(0)$ is bounded uniformly over $\mathbb{X}$. From (C.2) and (C.3) it follows easily that $x(0)$ is upper bounded uniformly over $\mathbb{X}$. We can also impose a (finite) lower bound for $x(0)$ without affecting the optimal solution because the value of the objective function goes to infinity as $x(0)$ approaches $-\infty$. This shows that the feasible region is essentially compact. The proof is thus complete. $\qquad \square$

Proof of Proposition 3.1. Suppose, by way of contradiction, that there exists another charging policy $\tilde{m}$

such that

$$\int_0^\tau p(t)\tilde{m}(t)dt < \int_0^\tau p(t)m^*(t)dt. \tag{C.5}$$

Then, from (12) it follows that

$$\tilde{m}(t) - m^*(t) = \begin{cases} \tilde{m}(t) - \kappa \leq 0 & \text{for} \quad t \in \phi(\zeta^*), \\ \tilde{m}(t) - 0 \geq 0 & \text{for} \quad t \notin \phi(\zeta^*). \end{cases} \tag{C.6}$$

Because $\phi \equiv \phi(\zeta^*)$ is the collection of time instances at which the electricity price p is less than or equal to ζ^*, we have

$$\int_0^\tau p(t)\tilde{m}(t)dt - \int_0^\tau p(t)m^*(t)dt = \int_\phi p(t)(\tilde{m}(t) - m^*(t))dt + \int_{\phi^c} p(t)(\tilde{m}(t) - m^*(t))dt. \tag{C.7}$$

Using (C.6), the right hand side of (C.7) is at least

$$\int_\phi \zeta^*(\tilde{m}(t) - m^*(t))dt + \int_{\phi^c} \zeta^*(\tilde{m}(t) - m^*(t))dt = \zeta^* \int_0^\tau \tilde{m}(t)dt - \zeta^* \int_0^\tau m^*(t)dt = 0, \tag{C.8}$$

for the last equality in (C.8) owing to (3). This implies

$$\int_0^\tau p(t)\tilde{m}(t)dt - \int_0^\tau p(t)m^*(t)dt \geq 0,$$

which contradicts the assumption (C.5). Hence, there is no feasible charging policy that can beat m^* in terms of minimizing the charging cost. $\qquad\square$

Proof of Theorem 3.3. Note that the first case follows directly from Proposition 3.1 and the construction (16) - (18). It remains to show the second case. Suppose for the sake of contradiction that there exists $b < b^*$ for which $(y(0), m^*)$ is an optimal solution. Then it must be the case that $y(t) \geq 0$ for all $0 \leq t \leq \tau$. Note that $x^*(0)$ in (16) is the smallest value that makes $x(t) \geq 0$ for $0 \leq t \leq \tau$. Therefore, $y(t) \geq 0$ implies $y(0) \geq x^*(0)$. Also note that y satisfies

$$y(t) = y(0) + \mu \int_0^t m^*(u)du - \Lambda(t). \tag{C.9}$$

Combining with (17) yields

$$y(t) - x^*(t) = y(0) - x^*(0) \geq 0 \quad \text{for all} \quad 0 \leq t \leq \tau. \tag{C.10}$$

To proceed, suppose the right hand side of (18) reaches its maximum at time u, i.e., $m^*(u) + x^*(u) = b^*$. Then

$$m^*(u) \leq b - y(u) < b^* - x^*(u) = m^*(u),$$

where the first inequality follows from the constraint (2d) and the assumption $y(t) \geq 0$ for all $0 \leq t \leq \tau$, the second inequality is due to (C.10) and the assumption $b < b^*$. But this leads to a contradiction and thus completes the proof. $\square$

Proof of Theorem 5.1. To reformulate the problem, we will need to analyze each constraint in (25) where uncertainty is involved, and determine its "worst-case scenario". Then we are guaranteed that the constraint is satisfied for any realization of the uncertainty. We start with the nonnegativity constraint, i.e., $\tilde{x}(t) \geq 0$. It is worthwhile to notice a straightforward fact about the realized FB inventory process:

$$\tilde{x}(t) = x_0 + \int_0^t (m(u) - \tilde{\lambda}(u))du = x(t) - \int_0^t z(u)du, \tag{C.11}$$

for

$$x(t) = x_0 + \int_0^t (m(u) - \lambda(u))du \quad \text{and} \quad z(t) \equiv \tilde{\lambda}(t) - \lambda(t).$$

Hence, to determine the worst-case scenario, it suffices to seek a realization of z that minimizes the right-hand side of (C.11); i.e., we need to find a realization of z that solves, for each $t \leq \tau$,

$$\max_z \quad \int_0^t z(u)du$$

$$\text{s.t.} \quad \int_0^t |z(u)|du \leq \Gamma(t) \quad \text{and} \quad 0 \leq |z(u)| \leq \hat{\lambda}(u) \quad \text{for all} \quad u \in [0, t].$$

It is immediate that at the optimal solution, $z \geq 0$. We can therefore rewrite the constraints on the variable z to obtain an equivalent problem

$$\max_z \quad \int_0^t z(u)du$$
$$\text{s.t.} \quad \int_0^t z(u)du \leq \Gamma(t) \quad \text{and} \quad 0 \leq z(u) \leq \hat{\lambda}(u) \quad \text{for all} \quad u \in [0, t]. \tag{C.12}$$

It turns out that problem (C.12) is a specific instance of the continuous linear program introduced by Bellman (2013), and we obtain strong duality and with its dual formulation provided below:

$$\min_{\omega(t), \gamma(\cdot, t)} \quad \omega(t)\Gamma(t) + \int_0^t \gamma(u, t)\hat{\lambda}(u)du$$
$$\text{s.t.} \quad \omega(t) + \gamma(u, t) \geq 1 \quad \forall u \in [0, t] \tag{C.13}$$
$$\omega(t) \geq 0 \quad \text{and} \quad \gamma(u, t) \geq 0 \quad \forall u \in [0, t].$$

The constraint $m(t) + \tilde{x}(t) \leq b$ can be analyzed in a similar fashion, and the determination of the worst-case scenario reduces to an optimization problem which is essentially the same as that in (C.12). As a consequence, their respective dual formulations are the same, as specified by (C.13). We observe that both

33

the primal (C.12) and its dual (C.13) take only the known parameters $\hat{\lambda}$ and Γ as inputs, and can be solved independently. We thus obtain the *modified* decision region defined through (26) with

$$\eta(t) \equiv \omega^*(t)\Gamma(t) + \int_0^t \gamma^*(u,t)\hat{\lambda}(u)du$$

for (ω^*, γ^*) being the solution to problem (C.13). Clearly, the first inequality constraint in (C.13) can be replaced by $\omega(t) + \gamma(u,t) = 1$. Upon substituting it into the objective function yields the desired result.

References

Amjady, N., Keynia, F., 2009. Day-ahead price forecasting of electricity markets by mutual information technique and cascaded neuro-evolutionary algorithm. IEEE Transactions on Power Systems 24, 306–318.

Bauer, G.S., Greenblatt, J.B., Gerke, B.F., 2018. Cost, energy, and environmental impact of automated electric taxi fleets in manhattan. Environmental Science & Technology 52, 4920–4928.

Bayram, I.S., Michailidis, G., Devetsikiotis, M., Granelli, F., 2013. Electric power allocation in a network of fast charging stations. IEEE Journal on Selected Areas in Communications 31, 1235–1246.

Beck, A., 2014. Introduction to Nonlinear Optimization: Theory, Algorithms, and Applications with MATLAB. volume 19. SIAM.

Bellman, R., 2013. Dynamic programming. Courier Corporation.

Bellos, I., Ferguson, M., Toktay, L.B., 2017. The car sharing economy: Interaction of business model choice and product line design. Manufacturing & Service Operations Management 19, 185–201.

Bertsekas, D.P., 1995. Dynamic programming and optimal control. volume 1. Athena Scientific Belmont, MA.

Bertsimas, D., Brown, D.B., Caramanis, C., 2011. Theory and applications of robust optimization. SIAM Review 53, 464–501.

Chung, H., Freund, D., Shmoys, D.B., 2018. Bike angels: An analysis of citi bike's incentive program, in: Proceedings of the 1st ACM SIGCAS Conference on Computing and Sustainable Societies, ACM. p. 5.

Diaz, A., Fu, M.C., 1997. Models for multi-echelon repairable item inventory systems with limited repair capacity. European Journal of Operational Research 97, 480–492.

Gnann, T., Funke, S., Jakobsson, N., Plötz, P., Sprei, F., Bennehag, A., 2018. Fast charging infrastructure for electric vehicles: Today's situation and future needs. Transportation Research Part D: Transport and Environment 62, 314–329.

Gross, D., Miller, D.R., Soland, R.M., 1983. A closed queueing network model for multi-echelon repairable item provisioning. AIIE Transactions 15, 344–352.

He, L., Mak, H.Y., Rong, Y., Shen, Z.J.M., 2017. Service region design for urban electric vehicle sharing systems. Manufacturing & Service Operations Management 19, 309–327.

Jie, W., Yang, J., Zhang, M., Huang, Y., 2019. The two-echelon capacitated electric vehicle routing problem with battery swapping stations: Formulation and efficient methodology. European Journal of Operational Research 272, 879–904.

Kurtz, T.G., et al., 1978. Strong approximation theorems for density dependent markov chains. Stochastic Processes and Their Applications 6, 223–240.

LCG Consulting, 2018. Energy Online. `http://www.energyonline.com/Data/GenericData.aspx?DataId=12&NYISO___Actual_Energy_Price`.

Liberzon, D., 2011. Calculus of variations and optimal control theory: a concise introduction. Princeton University Press.

Loeb, B., Kockelman, K.M., Liu, J., 2018. Shared autonomous electric vehicle (SAEV) operations across the austin, texas network with charging infrastructure decisions. Transportation Research Part C: Emerging Technologies 89, 222–233.

Maglaras, C., Meissner, J., 2006. Dynamic pricing strategies for multiproduct revenue management problems. Manufacturing & Service Operations Management 8, 136–148.

Mak, H.Y., Rong, Y., Shen, Z.J.M., 2013. Infrastructure planning for electric vehicles with battery swapping. Management Science 59, 1557–1575.

Mark Chediak, 2017. The Latest Bull Case for Electric Cars: the Cheapest Batteries Ever. `https://www.bloomberg.com/news/articles/2017-12-05/latest-bull-case-for-electric-cars-the-cheapest-batteries-ever`.

Nurre, S.G., Bent, R., Pan, F., Sharkey, T.C., 2014. Managing operations of plug-in hybrid electric vehicle (phev) exchange stations for use with a smart grid. Energy Policy 67, 364–377.

Riis, J.O., 1965. Discounted Markov programming in a periodic process. Operations Research 13, 920–929.

Schäl, M., 1993. Average optimality in dynamic programming with general state space. Mathematics of Operations Research 18, 163–172.

Schneider, F., Thonemann, U.W., Klabjan, D., 2017. Optimization of battery charging and purchasing at electric vehicle battery swap stations. Transportation Science 52, 1211–1234.

Sethi, S.P., Thompson, G.L., 2000. Dynamic programming and optimal control. Springer.

Sherbrooke, C.C., 1968. Metric: A multi-echelon technique for recoverable item control. Operations Research 16, 122–141.

Sun, B., Tan, X., Tsang, D.H.K., 2018a. Optimal charging operation of battery swapping and charging stations with qos guarantee. IEEE Transactions on Smart Grid 9, 4689–4701.

Sun, H., Yang, J., Yang, C., 2018b. A robust optimization approach to multi-interval location-inventory and recharging planning for electric vehicles. Omega .

Tan, X., Sun, B., Wu, Y., Tsang, D.H., 2017. Asymptotic performance evaluation of battery swapping and charging station for electric vehicles. Performance Evaluation 119, 43–57.

Whitt, W., 2006. Staffing a call center with uncertain arrival rate and absenteeism. Production and Operations Management 15, 88.

Widrick, R.S., Nurre, S.G., Robbins, M.J., 2018. Optimal policies for the management of an electric vehicle battery swap station. Transportation Science 52, 59–79.

Yang, J., Dong, J., Hu, L., 2017. A data-driven optimization-based approach for siting and sizing of electric taxi charging stations. Transportation Research Part C: Emerging Technologies 77, 462–477.

Zhang, X., Grijalva, S., 2015. An advanced data driven model for residential electric vehicle charging demand, in: Power & Energy Society General Meeting, 2015 IEEE, IEEE. pp. 1–5.